Aust. J. Phys., 1996, **49**, 499–514

New Data from Laser Interrogation of Electron–Atom Collisions Experiments*

A. T. Masters, R. T. Sang, W. R. MacGillivray and M. C. Standage

Laser Atomic Physics Laboratory, School of Science,
Griffith University, Nathan, Qld 4111, Australia.

Abstract

Recent data from two methods in which high resolution laser radiation is used to assist in determining electron–atom collision parameters are presented. The electron superelastic method has yielded the first measurement of Stokes parameters for electron de-excitation of the $3^2D_{5/2}$–$3^2P_{3/2,1/2}$ transition of atomic Na, the upper level having been optically prepared by resonant, stepwise excitation from the $3^2S_{1/2}$ ground level via the $3^2P_{3/2}$ level using two single mode lasers. As well, we report on the development of a model to determine the optical pumping parameters for superelastic scattering from the $3^2P_{3/2}$ level when it is prepared by two lasers exciting from the $F = 1$ and $F = 2$ states respectively of the $3^2S_{1/2}$ ground level. Data are also presented for collision parameters for the excitation of the 6^1S_0–6^1P_1 transition of the $I = 0$ isotope of Hg by electrons of 50 eV incident energy. The technique employed for these measurements is the stepwise electron–laser excitation coincidence method, in which the electron excited atom is further excited by resonant laser radiation, and fluorescence photons emitted by relaxation from the laser excited state are detected in coincidence with the scattered electron.

1. Introduction

The use of lasers as tools in the study of collisions between electrons and atoms is now well established. Techniques include the laser assisted excitation method, where the energy required to excite an atomic transition is provided by the absorption of a photon from a laser field simultaneously with the inelastic scattering of an electron (Newell 1992), and the photon recoil method (Jiang *et al.* 1992) in which the collision cross section is obtained by measuring the deflection of an atom in a beam following an elastic or inelastic collision with an electron and the transfer of momentum via resonant interaction with laser radiation.

More complete descriptions of electron–atom collisions can be obtained from correlation experiments, for example, a conventional coincidence experiment. In this type of study, the fluorescence photon emitted by an atom following excitation by an inelastic collision with an electron is detected in coincidence with the scattered electron. Not only can the magnitude but also the relative phase of the scattering amplitude a_m be determined from this experiment (see, for example, Andersen *et al.* 1988).

* Refereed paper based on a contribution to the Advanced Workshop on Atomic and Molecular Physics, held at the Australian National University, Canberra, in February 1995.

0004-9506/96/020499$05.00

The electron excited atomic state can be represented by the density matrix ρ whose elements ρ_{nm} are given by $\langle a_n a_m^* \rangle$. The complex matrix elements can be reformulated in terms of real parameters which can be measured directly in an experiment. Several parametrisations exist but we will confine ourselves to the 'collision frame' in which the quantisation axis is defined as the direction of the incident electron. For the excitation of an S–P transition, the parameters in this frame are defined as (Hertel and Stoll 1977)

$$\lambda = \frac{\rho_{00}}{\rho_{00} + 2\rho_{11}}, \quad \cos\chi = \frac{\mathrm{Re}(\rho_{10})}{(\rho_{00}\,\rho_{11})^{\frac{1}{2}}}, \quad \sin\phi = \frac{\mathrm{Im}(\rho_{10})}{(\rho_{00}\,\rho_{11})^{\frac{1}{2}}}, \quad \cos\delta = \frac{\rho_{1-1}}{\rho_{11}}. \quad (1)$$

It should be noted that the diagonal elements of the density matrix represent the substate populations of the P state or, in collision parlance, are partial differential cross sections. Here $\cos\chi$ and $\sin\phi$ contain phase information and $\cos\delta$ describes the breaking of the positive reflection symmetry about the scattering plane due to the flipping of the electron spin between the scattered and incident electrons. This spin flip can occur due to spin–orbit coupling between the incident electron and the atomic nucleus. In the absence of spin flip, $\cos\delta$ is -1.

The collision parameters can be deduced from the experiment by measuring the Stokes parameters of the time resolved fluoresence intensity of the coincidence signal. Stokes parameters completely describe the polarisation state of light and can be obtained from straightforward measurements of intensity (Born and Wolf 1975). In a geometry where the fluoresence is detected in a direction perpendicular to the scattering plane, defined as containing the incident and scattered electrons, the Stokes parameters are defined as

$$P_1 = \frac{I_0 - I_{90}}{I_0 + I_{90}}, \qquad P_2 = \frac{I_{45} - I_{135}}{I_{45} + I_{135}}, \qquad P_3 = \frac{I_{\mathrm{RHC}} - I_{\mathrm{LHC}}}{I_{\mathrm{RHC}} + I_{\mathrm{LHC}}}, \quad (2)$$

where the subscripts of the intensity I denote either the transmission through a linear polariser at angle β to the incident electron direction or the handedness of a $\lambda/4$ plate through which the fluorescence photons pass.

For the case of no spin flips, it can be shown that the Stokes parameters are related to the collision parameters by

$$P_1 = 2\lambda - 1, \qquad P_2 = -2[\lambda(1-\lambda)]^{\frac{1}{2}}\cos\chi, \qquad P_3 = 2[\lambda(1-\lambda)]^{\frac{1}{2}}\sin\phi. \quad (3)$$

Also, a measure of the coherence of the collision process can be obtained from the Stokes parameters by forming the degree of polarisation P_{TOT},

$$P_{\mathrm{TOT}} = (P_1^2 + P_2^2 + P_3^2)^{\frac{1}{2}}. \quad (4)$$

If spin flips cannot be ignored, a fourth measurement is required to obtain $\cos\delta$. In the conventional coincidence experiment, $\cos\delta$ is found by determining the P_1 Stokes parameter for fluoresence scattered in the scattering plane. This parameter is usually denoted as P_4. Equation (4) is still applicable by restricting its meaning to terms with positive reflection symmetry about the scattering plane (Andersen *et al.* 1988).

Laser radiation does not feature in the conventional coincidence experiment. However, there are two current methods, electron superelastic scattering and stepwise coincidence, which do involve the use of lasers to measure the collision parameters.

The electron superelastic scattering method (see, for example, Hertel and Stoll 1977) is essentially the time reverse process of the conventional coincidence experiment in that the atom is first excited by absorbing laser radiation of known polarisation followed by radiationless relaxation due to a collision with an electron. Those electrons which have gained energy and have scattered at a particular angle are detected and their differential cross section S measured as a function of laser polarisation. The cross section S can be written as the product of two density matrices,

$$S = \sum_{mn} \rho^{\mathrm{L}}_{mn}\, \rho_{mn}\,, \tag{5}$$

where the density matrix elements ρ^{L}_{mn} and ρ_{mn} describe the laser and electron excitation of the transition respectively. Equation (5) can be interpreted as the overlap between the two excitation processes.

Pseudo Stokes parameters are defined in terms of the values of S measured as a function of the polarisation of the incident laser,

$$P^{\mathrm{S}}_1 = \frac{S_0 - S_{90}}{S_0 + S_{90}}, \qquad P^{\mathrm{S}}_2 = \frac{S_{45} - S_{135}}{S_{45} + S_{135}}, \qquad P^{\mathrm{S}}_3 = \frac{S_{\mathrm{RHC}} - S_{\mathrm{LHC}}}{S_{\mathrm{RHC}} + S_{\mathrm{LHC}}}\,, \tag{6}$$

where the subscripts on S have the same meaning as those for I in equation (2). For the reverse of the system described by equations (2) and (3), that is, superelastic scattering from a P state prepared by laser excitation from an S state for an atom for which LS coupling holds and there are no spin flips, the pseudo Stokes parameters can be related to the Stokes parameters of equation (3) by (Farrell *et al.* 1991)

$$P^{\mathrm{S}}_1 = KP_1, \qquad P^{\mathrm{S}}_2 = KP_2, \qquad P^{\mathrm{S}}_3 = K'P_3\,, \tag{7}$$

where K and K' describe the optical pumping of the excited state by linearly (π excitation) and circularly (σ excitation) polarised light respectively. If the states involved in the transition were pure S and L states, K and K' would both be unity. An illustration of such a system is the recent work of Law and Teubner (1993) on the 4^1S–4^1P transition of Ca. However, where the levels have fine or hyperfine structure as in the well studied case of the D_2 line of Na, K and K' are no longer constant and their values depend on such quantities as the intensity and detuning of the laser field and the dipole moment induced between substates of the upper and lower states.

A full quantum electrodynamic (QED) theory (Farrell *et al.* 1991) has been developed for the calculation of K and K'. The model is derived in terms of the atomic operator $\bar{\sigma}$ which has elements

$$\sigma_{ij} = |i\rangle\langle j|\,. \tag{8}$$

At time t, the expectation value of atomic operator elements and density matrix elements are related by

$$\langle \sigma_{ij}(t) \rangle = \rho_{ji}(t) \,. \tag{9}$$

The parameters K and K' can be evaluated from the atomic operator elements. In fact, since K and K' are real quantities, their expressions in terms of $\langle \sigma_{ij}(t) \rangle$ and ρ_{ij}^{L} (t) are identical. The time evolution of $\bar{\sigma}$ is governed by the Heisenberg equation of motion

$$\dot{\bar{\sigma}} = \frac{i}{\hbar} \left[\bar{H}, \bar{\sigma} \right], \tag{10}$$

where $\bar{H}$ is the fully quantum mechanical Hamiltonian which describes the atom–light interaction (Farrell *et al.* 1988).

The parameters K and K' have been calculated for the $3^2\mathrm{S}_{1/2}(F=2)$–$3^2\mathrm{P}_{3/2}(F=3,2,1)$ hyperfine transitions of Na using the QED model and their dependence on laser intensity and detuning investigated (Farrell *et al.* 1991). More recently, the QED model has been employed to calculate the optical pumping parameters for transitions in Li (Farrell 1994) and Rb (Hall *et al.* 1995). In Section 2, we report on the extension of the Na model to include a second laser mode to excite the $3^2\mathrm{S}_{1/2}(F=1)$–$3^2\mathrm{P}_{3/2}(F=2,1,0)$ transitions simultaneously with the transitions from the $F=2$ ground state. Also in Section 2, we report preliminary data from a stepwise experiment where electrons are superelastically scattered from the $3^2\mathrm{D}_{5/2}$ state of Na which is optically prepared by excitation from the $3^2\mathrm{S}_{1/2}$ ground state via the $3^2\mathrm{P}_{3/2}$ state by resonant radiation from two lasers.

The stepwise electron–laser excitation coincidence method was developed (Murray *et al.* 1989) to access electron excited transitions not suitable for study by either the conventional coincidence or the superelastic scattering methods. An example of such a transition is electron excitation to a metastable state from which no fluorescence is possible. Another example is of a transition which is in part of the spectrum, such as the vacuum ultraviolet, for which a suitable laser source has not been developed and for which optical elements and detectors are very inefficient. The stepwise method involves further exciting the atom with resonant laser radiation after an inelastic electron collision. Since the laser excitation process is coherent, the information concerning the electron excitation contained in the intermediate state is transferred to the laser excited state. Fluorescence photons from the laser excited state emitted during relaxation in an appropriate channel are detected in coincidence with the scattered electron. The Stokes parameters of the time integrated coincidence signal are measured.

This technique has been proven by measuring the collision parameters for the electron excitation of the $6^1\mathrm{S}_0$–$6^1\mathrm{P}_1$ transition of mercury at 185 nm. The Hg energy level scheme and the experimental geometry used are shown in Fig. 1. Resonant, single mode laser radiation at 579 nm excites the $6^1\mathrm{P}_1$–$6^1\mathrm{D}_2$ transition and fluorescence from the $6^1\mathrm{D}_2$–$6^3\mathrm{P}_1$ transition at 313 nm is detected. The problem of detecting and analysing photons in difficult regimes is alleviated somewhat by transferring the wavelength of the fluorescence to be monitored

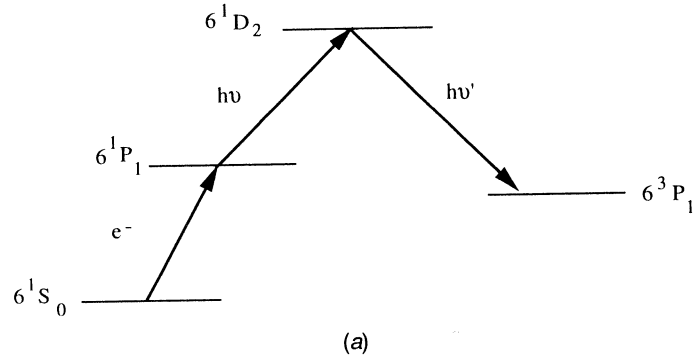

(a)

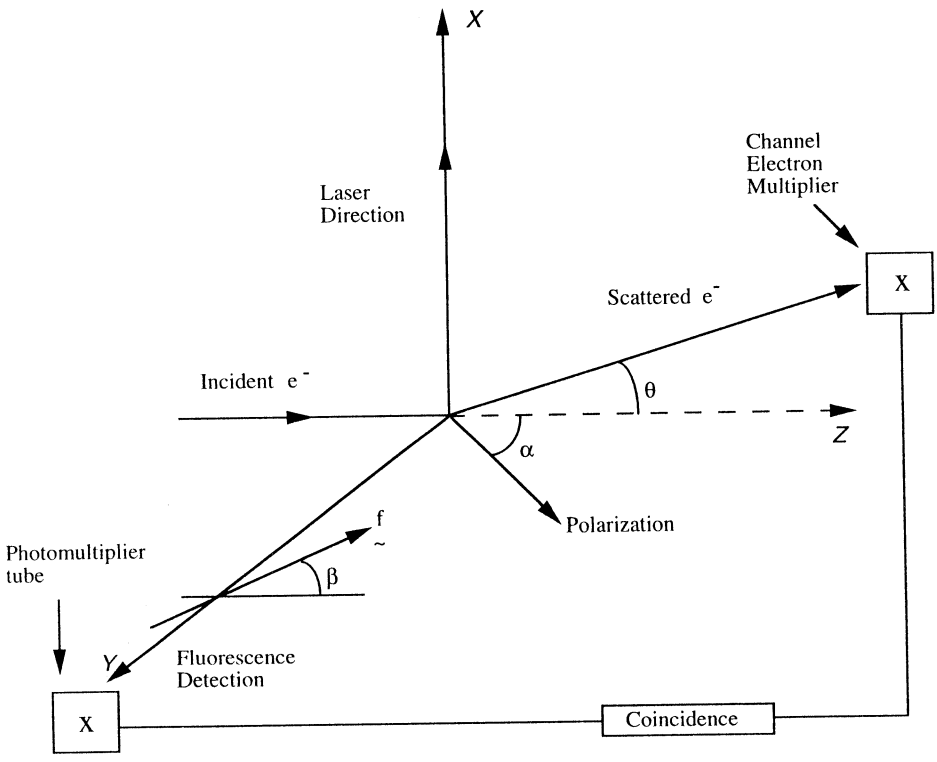

(b)

Fig. 1. Schematic diagram for (*a*) the process and (*b*) the experimental geometry used for the stepwise electron–laser excitation coincidence method of collision parameter measurement.

from the 185 nm of the 6^1S_0–6^1P_1 transition to the 313 nm of the 6^1D_2–6^3P_1 line. Further, the laser radiation is able to resolve the hyperfine structure in the 6^1P_1–6^1D_2 transition due to the various isotopes. Thus, measurements are able to be confined to the $I = 0$ isotope which has no hyperfine structure. The down side of mercury, however, is that *LS* coupling does not hold and so the states are

not pure singlet or triplet states but rather a mixture. Spin–orbit interactions also allow the potential for spin flip of the scattered electron so that all four collision parameters have to be measured.

If the laser radiation exciting the transition is weak, then the density matrix elements representing the laser excited state can be expressed in terms of the density matrix elements describing the electron excited state using the dipole approximation for the transition operator (MacGillivray and Standage 1988). The weak excitation approximation is valid if, during the entire excitation–deexcitation cycle, the atom absorbs no more than one photon from the laser field. In the weak excitation approximation, the Stokes parameters measured for the fluorescence from the laser excited state can be expressed explicitly in terms of the electron–atom collision parameters for the 6^1S_0–6^1P_1 excitation. For the collision frame parameters, the relationships are

$$IP_{1\alpha} = \lambda(\tfrac{27}{2} - 6\cos^2\alpha) + \tfrac{9}{2}\cos 2\alpha + \tfrac{9}{2}(1-\lambda)\cos\delta\,, \tag{11a}$$

$$IP_{2\alpha} = -3(5 - \cos 2\alpha)[\lambda(1-\lambda)]^{1/2}\cos\chi\,, \tag{11b}$$

$$IP_{3\alpha} = 9(3 + \cos 2\alpha)[\lambda(1-\lambda)]^{1/2}\sin\phi\,, \tag{11c}$$

$$I = \lambda(6\cos^2\alpha + \tfrac{1}{2}) + (5\cos^2\alpha + \tfrac{17}{2}) + \tfrac{1}{2}(1-\lambda)(8\sin^2\alpha - 9)\cos\delta\,, \tag{11d}$$

where α is the angle that the laser polarisation makes with the quantisation axis as shown in Fig. 1. Here α is an additional experimental variable which is not available in the conventional coincidence method. This angle allows the full determination of the collision parameters from the Stokes parameters measured perpendicular to the scattering plane, that is, no P_4 measurement of fluorescence emitted in the scattering plane needs to be performed. For example λ and $\cos\delta$ can be evaluated from equation (11a) by making measurements with α set at 0° and 90°. Then $\cos\chi$ and $\sin\phi$ are obtained from equations (11b) and (11c) respectively for α set to 0°.

Collision data for electrons of 16 eV incident energy have been previously reported for scattering angles to 30° (Murray *et al.* 1992). It was noted that agreement with available theoretical calculations was poor for most of the parameters. In Section 3, we present the latest measurements from this experiment with electrons of incident energies of 50 eV.

2. Superelastic Scattering Method

(2a) Modelling of Optical Pumping Parameters for Two Mode Excitation of the $3^2S_{1/2}(F = 2, 1)$ $-^2P_{3/2}(F = 3, 2, 1, 0)$ Transitions of Na

Measurements of superelastic electron scattering from the $3^2P_{3/2}$ level of atomic sodium have been performed repeatedly since the initial experiment verifying the technique in the early 1970s (Hertel and Stoll 1974). The reason for the popularity of this system is the strength of the transition and its accessibility by dye lasers using Rhodamine 590 dye. Until recently, all of the experiments have involved excitation from the $3^2S_{1/2}(F = 2)$ ground state only since the

two ground hyperfine states cannot be excited simultaneously due to their frequency splitting of 1·772 GHz. However, even with the laser tuned to the $3^2S_{1/2}(F=2)$–$3^2P_{3/2}(F=3)$ transition, power broadening by the radiation and Doppler shifting due to atomic motion can populate the $F=2$ excited state which is split from the $F=3$ state by 59·5 MHz. Even the $F=1$ excited state with a splitting of 36·5 MHz from the $F=2$ state may be excited. Both the $F=2$ and $F=1$ excited states can relax to the $F=1$ ground state which then acts as a sink removing atoms from the excitation process.

There are several ways of overcoming this problem. Firstly, the atomic beam can be produced so that it has a high degree of collimation with a residual Doppler width that is much less than the splitting of the $F=3$ and $F=2$ excited states. Then the intensity of the laser radiation must be maintained below that which would lead to a power broadening of the absorption profile of 60 MHz. While both of these requirements are technically achievable, calculations show that the value of the optical pumping parameter K varies rapidly with both laser detuning and intensity under these conditions (Farrell *et al.* 1991). Our experiments have been performed using an atomic beam with a 300 MHz Doppler width under which condition the value of K remains almost constant above a particular laser intensity. The disadvantage of such a beam is that the excited state population is severely limited by losses to the $F=1$ ground state. This had the consequence of limiting the scattering angle measurements for P_1^S and P_2^S to 15° or less where the signal-to-noise ratio for the superelastic signal was sufficient. [The problem of the $F=1$ ground state sink does not exist to the same extent for P_3^S measurements since the circularly polarised light pumps the atom to the 'two level' transition of $3^2S_{1/2}(F=2,m_F=2)$–$3^2P_{3/2}(F=3,m_F=3)$ or the equivalent negative m_F values for the other handedness, from which it is not possible for the atom to relax to the $F=1$ ground state.]

Our approach to the problem of the $F=1$ ground state sink has been to utilise radiation from a second dye laser, tuned to excite the atoms from this state to the $3^2P_{3/2}$ excited level. In this way, no atoms are lost from the excitation process and the excited level population can be increased considerably resulting in a much higher signal-to-noise ratio for the superelastic scattering signal.

We have extended the QED model for laser excitation of the Na D_2 line to include the second field mode. Fig. 2 illustrates the effect of introducing the repumping laser from the $F=1$ ground state. Fig. 2*a* shows the total population probability for the $3^2P_{3/2}$ excited level for π excitation by a single laser tuned to the $3^2S_{1/2}(F=2)$–$3^2P_{3/2}(F=2)$ transition. Each ground substate has an initial population probability of 0·125 and the laser is assigned an intensity of 80 mW mm^{-2}. The sink effect of the $F=1$ ground state is clear as the excited level population goes to zero. The initial oscillations in the population are due to the complicated interplay of Rabi cycling in each participating hyperfine transition. When the second laser is introduced tuned to the $3^2S_{1/2}(F=1)$–$3^2P_{3/2}(F=2)$ transition, the excited level population no longer tends to zero as shown in Fig. 2*b*. The same substate initial populations are assumed and the intensity of the laser radiation exciting out of the $F=2$ ground state is maintained at 80 mW mm^{-2}. The intensity of the $F=1$ exciting laser is 10 mW mm^{-2} and its polarisation is assumed to be parallel to that of the first laser. This low intensity is clearly sufficient to counter the sink action of relaxation to the $F=1$

ground state. The total excited state population tends to 50% for long times which is the same as achieved in a simple two level system of one ground and one excited state. For the two field mode case, it is assumed that they originate from different lasers and so are not phase related.

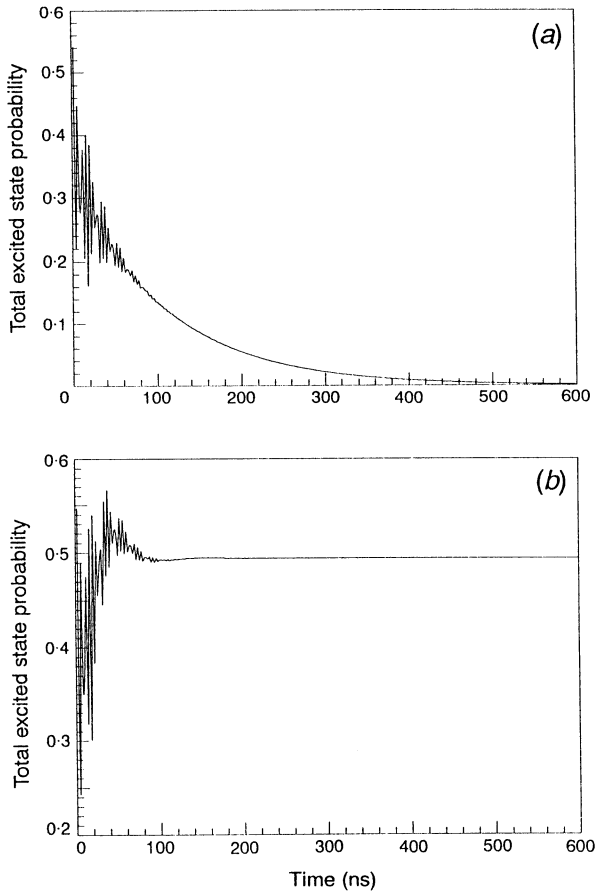

Fig. 2. The effect of repumping out of the $F = 1$ ground state. (a) Total population probability for the $3^2P_{3/2}$ level for π excitation from the $3^2S_{1/2}(F = 2)$ ground state with a laser intensity of 80 mW mm^{-2} tuned to the $3^2S_{1/2}(F = 2)$–$3^2P_{3/2}(F = 2)$ transition. (b) As for (a), but with addition of 10 mW mm^{-2} of laser radiation tuned to the $3^2S_{1/2}(F = 1)$–$3^2P_{3/2}(F = 2)$ transition.

Equations (7) are still appropriate for this folded step excitation scheme although the functional form of the optical pumping parameter K is different. For the folded step excitation scheme, the optical pumping parameter is denoted by $\bar{K}$. In Fig. 3, the calculated value of $\bar{K}$ is plotted as a function of the square root of the intensity of one exciting laser while the intensity of the other laser is held constant. The intensities are expressed in terms of the Rabi frequency of the $3^2S_{1/2}(F = 2, m_F = 0)$–$3^2P_{3/2}(F = 3, m_F = 0)$ transition which is the strongest in the manifold for π excitation. To represent the passage of the atoms through

the laser beams, the values of the operator elements are time-averaged over 1 μs. For two of the calculated curves, the $F = 1$ exciting laser is maintained at a constant intensity of 150 MHz on the scale used (approximately 40 mW mm^{-2}). Here $\overline{K}$ is calculated for both zero Doppler width of the atomic absorption profile and a Doppler width of 300 MHz. Both cases show similar behaviour with the zero Doppler width having the greater variation. The third curve depicts the variation of $\overline{K}$ with Rabi frequency for the $F = 1$ exciting laser while the $F = 2$ exciting laser is kept constant at 170 MHz (60 mW mm^{-2}). The calculation is for zero Doppler width and it can be seen that the variation of $\overline{K}$ is not as great as for the equivalent case where the intensity of the $F = 2$ exciting laser is varied.

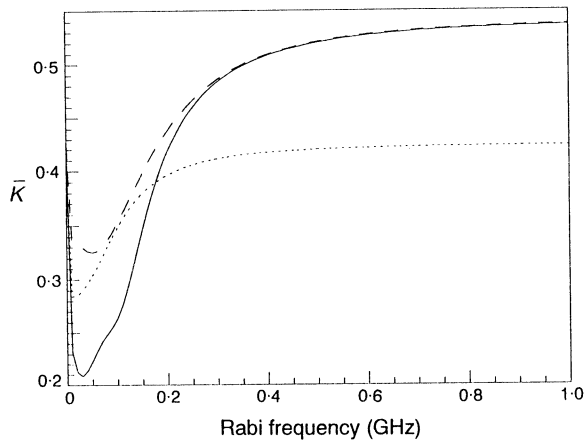

Fig. 3. Calculated values of $\overline{K}$ plotted as a function of laser intensity expressed in terms of the Rabi frequency of the $3^2S_{1/2}(F = 2, m_F = 0)$–$3^2P_{3/2}(F = 3, m_F = 0)$ transition. The lasers are tuned to the $3^2S_{1/2}(F = 2)$–$3^2P_{3/2}(F = 2)$ and $3^2S_{1/2}(F = 1)$–$3^2P_{3/2}(F = 2)$ transitions respectively: —— $F = 1$ exciting laser constant intensity, zero Doppler width; ------ $F = 1$ exciting laser constant intensity, 300 MHz Doppler width; and ····· $F = 2$ exciting laser constant intensity, zero Doppler width.

Measurements involving electron superelastic scattering from the $3^2P_{3/2}$ level of Na excited from both states of the $3^2S_{1/2}$ ground level by radiation from two lasers have been performed recently (Sang *et al.* 1994). Values for P_1^S and P_2^S at electron scattering angles of greater than 15° were able to be obtained.

(2b) Electron Superelastic Scattering from the $3^2D_{5/2}$ Level of Na

We have employed the superelastic scattering method to perform measurements of pseudo Stokes parameters for electron excitation of a channel that does not involve a ground state. Two lasers with parallel polarisations stepwise excited the $3^2D_{5/2}$ level via the resonant intermediate $3^2P_{3/2}$ level. The first excitation step is the D_2 line already studied and is excited by a dye laser operating in the visible at a vacuum wavelength of 589·16 nm. The upper transition was excited by a Ti:sapphire ring laser operating at a vacuum wavelength of 819·711 nm. The lasers were injected into the interaction region in counterpropagating directions.

The experimental protocol was similar to the single step superelastic scattering experiments (see, for example, Sang *et al.* 1994) and details are given elsewhere (Sang 1995).

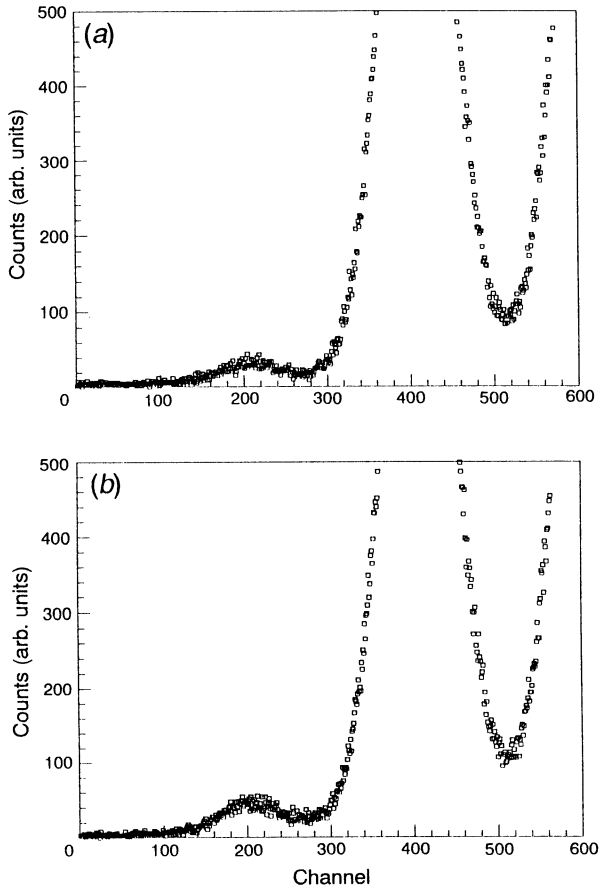

Fig. 4. Electron energy gain/loss spectra for sodium for 20 eV incident electrons: (*a*) atoms optically excited to the $3^2P_{3/2}$ level; (*b*) atoms optically excited to the $3^2P_{3/2}$ and $3^2D_{5/2}$ levels.

The energy gaps between the $3^2S_{1/2}$ and the $3^2P_{3/2}$ levels and the $3^2P_{3/2}$ and $3^2D_{5/2}$ levels are 2·1 and 1·6 eV respectively. With the electron gun and analyser used in the experiment, these two superelastic peaks cannot be resolved. Fig. 4*a* is an electron energy gain/loss spectrum for Na excited to the $3^2P_{3/2}$ level only for incident electrons of 20 eV energy. The peak centred on Channel 400 is the elastic scattering peak and the edge of the first inelastic peak appears at higher channel numbers. The peak at lower channels represents the detection of electrons superelastically scattered from the $3^2P_{3/2}$ level. Fig. 4*b* is an energy gain/loss spectrum when both lasers excite the atoms. The figure shows an increase in the number of superelastic counts and a broadening of the feature due to the convolution of the two superelastic scattering processes, $3^2P_{3/2}$ to $3^2S_{1/2}$ and

$3^2D_{5/2}$ to $3^2P_{3/2,1/2}$. Data for the latter process were collected by subtracting counts for the infrared laser blocked from those obtained when both lasers were injected. This is only an approximate method for obtaining the superelastic counts for the upper transition since the population of the $3^2P_{3/2}$ intermediate state will be reduced by excitation to the $3^2D_{5/2}$ state with a corresponding reduction of the superelastic count for the lower transition. However, a simple rate equation model of this process indicates that the population of the $3^2P_{3/2}$ state is reduced by less than 20%.

Table 1. Pseudo Stokes parameters for the $3^2D_{5/2}$–$3^2P_{3/2,1/2}$ transition of sodium measured by the electron superelastic scattering technique for 20 eV incident electrons

Scattering angle	P_1^S	P_2^S	P_3^S
10°	−0·23±0·04	0·10±0·02	−0·25±0·02
15°	−0·065±0·04	0·043±0·04	−0·41±0·02
18°			−0·22±0·04

Measured values for pseudo Stokes parameters for electron de-excitation of the $3^2D_{5/2}$ to $3^2P_{3/2,1/2}$ channel for parallel laser polarisations and 20 eV impact electrons are given in Table 1. These preliminary data are not sufficient to obtain a complete description of the collision process since the D state has a value of angular momentum of $l = 2$ as opposed to the P state previously studied which has $l = 1$. For the latter case, as represented by equation (1), four parameters are required to describe the S–P collision, or three if LS coupling holds and there are no spin flips. Twice the number of parameters are required to describe the P–D excitation. Extending the concepts of Blum (1981) and Nienhuis (1980), the density matrix representing the D state may be parametrised as (Sang 1995)

$$\lambda = \frac{\rho_{00}}{\sigma}, \qquad \mu = \frac{2\rho_{11}}{\sigma}, \tag{12a, b}$$

$$\cos\chi = \frac{\mathrm{Re}\rho_{10}}{(\rho_{11}\,\rho_{00})^{\frac{1}{2}}}, \qquad \sin\phi = \frac{\mathrm{Im}\rho_{10}}{(\rho_{11}\,\rho_{00})^{\frac{1}{2}}}, \tag{12c, d}$$

$$\cos\psi = \frac{\mathrm{Re}\rho_{21}}{(\rho_{22}\,\rho_{11})^{\frac{1}{2}}}, \qquad \sin\xi = \frac{\mathrm{Im}\rho_{21}}{(\rho_{22}\,\rho_{11})^{\frac{1}{2}}}, \tag{12e, f}$$

$$\cos\delta = \frac{\rho_{1-1}}{\rho_{11}}, \qquad \cos\eta = \frac{\rho_{2-2}}{\rho_{22}}, \tag{12g, h}$$

where $\sigma = \rho_{00}+2\rho_{11}+2\rho_{22}$ is the total differential cross section. Here 'Re' and 'Im' represent the real and imaginary part of the element respectively, while $\cos\delta$ and $\cos\eta$ are the spin-flip parameters and can be assumed to take on the values of -1 and 1 respectively for Na. This leaves six parameters required to characterise the D state. The three pseudo Stokes parameters measured for parallel laser polarisations are related to the collision parameters of equations (12) by (Sang 1995)

$$P_1^{\mathrm{S}} = \frac{(K_{\mathrm{n}} - 6)(3 - 3\mu - 6\lambda - 2\Lambda)}{(5K_{\mathrm{D}} + 18) + (54K_{\mathrm{D}} - 1)\frac{1}{2}\mu - (7K_{\mathrm{D}} + 6)\lambda + (K_{\mathrm{D}} - 6)2\Lambda}, \tag{13a}$$

$$P_2^{\mathrm{S}} = \frac{(K_{\mathrm{D}} - 6)\{6\cos\psi[\mu(\mu - \lambda - 1)]^{\frac{1}{2}} + 2\sqrt{3}\cos\chi[\lambda(1 - \lambda)]^{\frac{1}{2}}\}}{(\frac{25}{2}K_{\mathrm{D}} + 13) + (\frac{101}{2}K_{\mathrm{D}} + 41)\lambda - (\frac{29}{2}K_{\mathrm{D}} - 49)\mu - (13K_{\mathrm{D}} + 2)\Lambda}, \tag{13b}$$

$$P_3^{\mathrm{S}} = \frac{4\{\sin\xi[\mu(\mu - \lambda - 1)]^{\frac{1}{2}} + \sqrt{3}\sin\phi[\lambda(1 - \lambda)]^{\frac{1}{2}}\}}{1 + 2\lambda + 3\mu - 2\Lambda}, \tag{13c}$$

where Λ is defined as

$$\Lambda = \sqrt{3}\cos(\chi + \psi)[\lambda(1 - \mu - \lambda)]^{\frac{1}{2}} \tag{14}$$

and K_{D} is an optical pumping parameter for π excitation in the J representation given by

$$K_{\mathrm{D}} = \frac{\rho_{\frac{3}{2}\frac{3}{2}}}{\rho_{\frac{1}{2}\frac{1}{2}}}. \tag{15}$$

That is, K_{D} describes the relative populations of the $m_J = \frac{3}{2}$ and $m_J = \frac{1}{2}$ substates in the $3^2\mathrm{D}_{5/2}$ state after π excitation from the $3^2\mathrm{S}_{1/2}$ ground state via the resonant intermediate $3^2\mathrm{P}_{3/2}$ state.

It is clear from equations (13) that the measurement of these Stokes parameters is insufficient to extract values for all six collision parameters. In fact, six independent measurements are required. Further independent measurements can be achieved by choosing other geometries for the laser polarisations and/or propagation directions. However, these preliminary measurements of Stokes parameters demonstrate the feasibility of obtaining collision parameters for high lying atomic states using the electron superelastic scattering technique.

3. Stepwise Electron–Laser Excitation Coincidence Measurements for Hg

The mutually orthogonal geometry of Fig. 1*b* has been used to perform stepwise electron–laser excitation coincidence measurements on the Hg scheme of Fig. 1*a* for incident electrons of 50 eV energy. Details of the experimental apparatus have been given previously (Murray *et al.* 1992). The interaction region is created by the intersection of the atomic, electron and laser beams. The laser beam, having the smallest diameter of the three, effectively defines the stepwise interaction region which is approximately 1 mm^3. Typically, the laser power in the interaction region is 300 mW. Count rates from the electron and photon detectors are adjusted to give the best signal-to-noise ratio and smallest statistical error in the coincidence peak. An example of the rates is 7 kHz for the electrons and 400 Hz for the photons at 10° scattering angle. The vacuum chamber pressure is typically 4×10^{-6} mbar. Radiation trapping can occur in the interaction region and the data are corrected for this effect using a recently developed model (Masters *et al.* 1995).

The oscillator strength of the $6^1\mathrm{P}_1$–$6^1\mathrm{D}_2$ transition is quite weak. Further, the lifetime of the $6^1\mathrm{P}_1$ state (1·2 ns) is an order of magnitude smaller than the laser excited $6^1\mathrm{D}_2$ state. Atoms returning to the $6^1\mathrm{P}_1$ state either by spontaneous or

stimulated emission from the upper state are far more likely to relax to the 6^1S_0 ground state than to be re-excited to the 6^1D_2 state. Under these conditions, the weak excitation approximation is good and equations (11) hold (Murray *et al.* 1990).

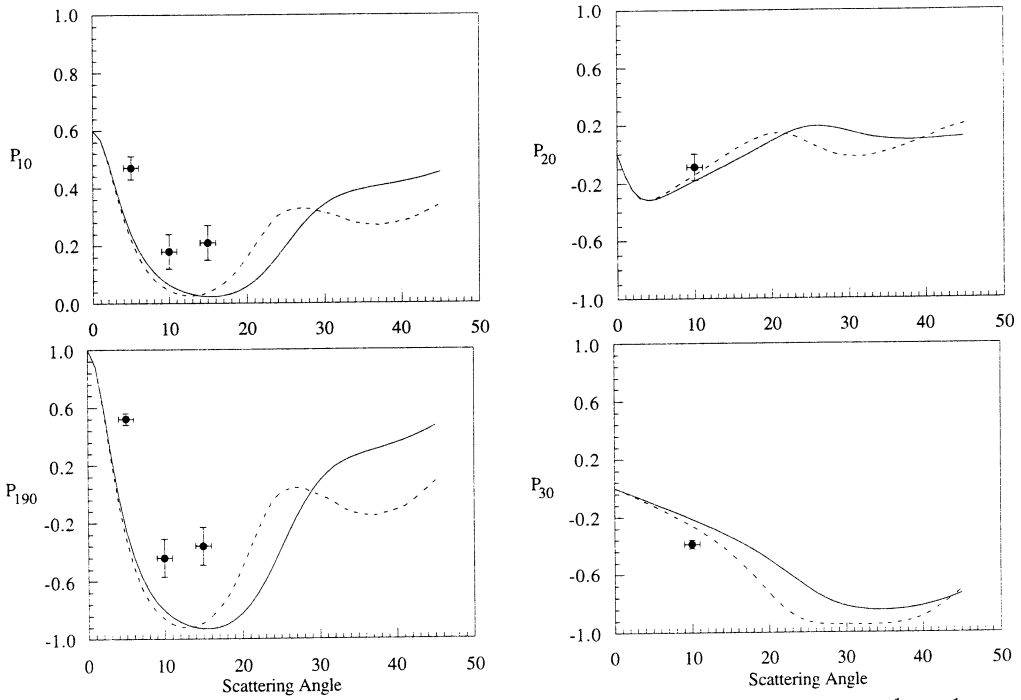

Fig. 5. Stepwise coincidence Stokes parameters for electron excitation of the 6^1S_0–6^1P_1 ($I = 0$) transition of mercury by 50 eV incident electrons. The Stokes parameters are for the fluorescence channel 6^1D_2–6^3P_1 where the upper state has been excited from the electron excited state by single mode laser radiation at 579 nm. The theoretical curves are plotted from the data of Madison (1994) (------) and McEachran (1994) (——).

Stepwise coincidence Stokes parameters have been measured for scattering angles of 5°, 10° and 15°. The scattering angles are defined with an error of 1°. The input aperture to the electron analyser that detects the scattered electrons defines a solid angle of $7{\cdot}66\times10^{-4}$ sr, while for the fluorescence collecting lens the solid angle is 0·51 sr. The small acceptance angle of the electron detector reduced the effect of correction due to the finite volume of the interaction region (Murray *et al.* 1992) below the statistical error for all measurements. Fig. 5 displays stepwise coincidence Stokes parameters, as defined by equations (11) with $\alpha = 0°$ and 90°, corrected for radiation trapping. The vertical error bars are the statistical estimate of one standard deviation, while the horizontal bars indicate the error in the value of the scattering angle. The experimental data are compared with theoretical calculations by Madison (1994) and McEachran (1994) using second order distorted wave Born approximation (DWBA2) models (Bartschat and Madison 1987; Zuo *et al.* 1991; Srivastava *et al.* 1992). For each of the theoretical models, the atomic wavefunctions used in the calculations are generated from the Dirac equation. While McEachran employs the full relativistic solution for the wavefunctions, Madison uses only the large component leading

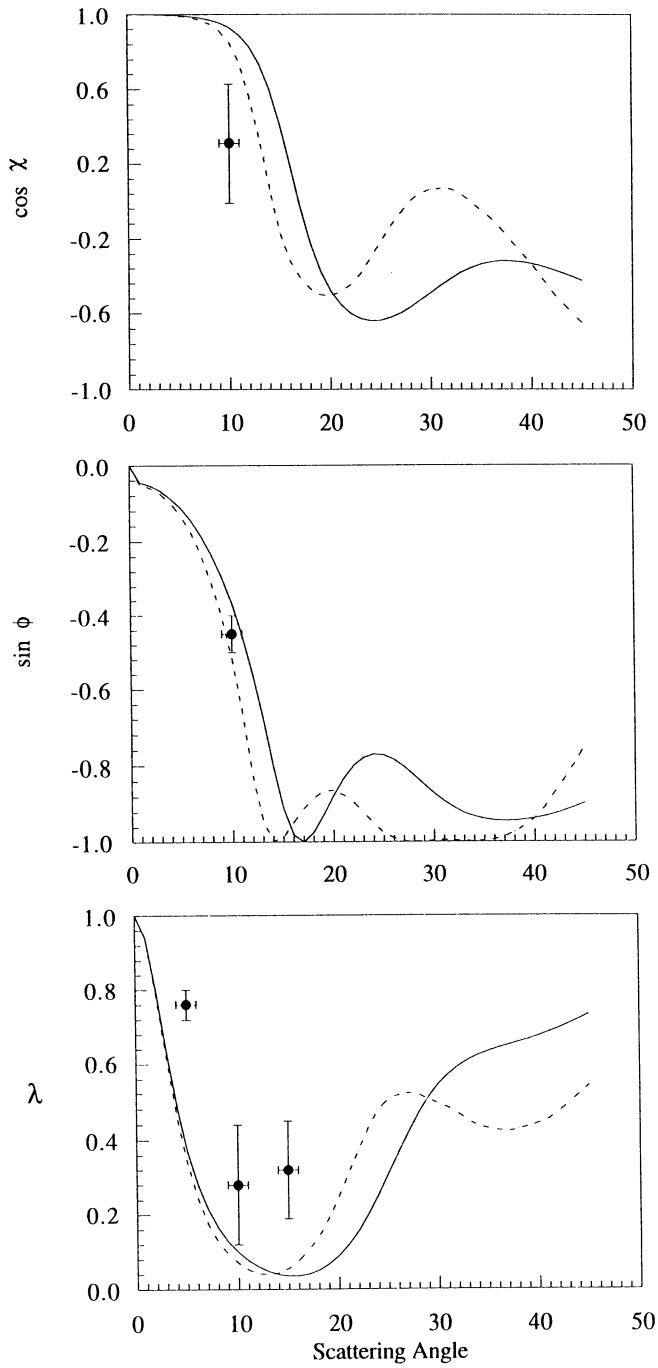

Fig. 6. Collision frame parameters for the excitation of the 6^1S_0–6^1P_1 ($I = 0$) transition of mercury by electrons of incident energy of 50 eV. The theoretical curves are plotted from the data of Madison (1994) (------) and McEachran (1994) (——).

to a semi-relativistic calculation. For P_{10} and P_{190}, while there is not absolute agreement, the experimental and theoretical data demonstrate the same features at the low scattering angles. The single measurements at 10° of P_{20} and P_{30} lie close to each of the theoretical curves.

The corresponding collision frame parameters are plotted together with the theoretical data in Fig. 6. The raw data for $\cos\delta$ were consistent with their having the value of -1 at these angles. Thus, for the calculations which corrected for the effect of radiation trapping, $\cos\delta$ was assumed to be -1. The implication of the absence of spin-flips at these scattering angles is understood when it is realised that electrons scattered in the forward direction have not approached the nucleus closely and so have little chance of spin–orbit interaction. The measured values of λ are larger than the theoretical calculations but indicate the same form of angular dependence. The measured $\cos\chi$ has a large uncertainty but lies close to the theoretical curves, while $\sin\phi$ shows good agreement with the theory. This latter parameter represents the transfer of angular momentum to the atom and, at 16 eV, was very small at all scattering angles measured to 30° (Murray *et al.* 1992) and, subsequently, was at variance with the theoretical calculations. For the 50 eV case presented here, both the experiment and theory yields similar nonzero values for $\sin\phi$ at 10°.

The approximations inherent in the DWBA2 models make them more accurate at intermediate electron energies and above so their failure to agree with the 16 eV data is perhaps not surprising. On the other hand, it is encouraging that the experimental data obtained so far at 50 eV display quite good agreement with the calculations. We are currently extending the measurements at 50 eV to other scattering angles and have commenced measurements at 100 eV.

Acknowledgments

The work reported here has been funded chiefly through the Australian Research Council. One of us (RTS) acknowledges the support of an Australian Postgraduate Research Award. The authors wish to thank Professors Don Madison and Bob McEachran for providing data from their calculations.

References

Andersen, N., Gallagher, J. W., and Hertel, I. V. (1988). *Phys. Rep.* **165**, 1.
Bartschat, K., and Madison, D. H. (1987). *J. Phys.* B **20**, 1609.
Blum, K. (1981). 'Density Matrix Theory and Applications' (Plenum: New York).
Born, M., and Wolf, E. (1975). 'Principles of Optics' (Oxford: Pergamon).
Farrell, P. M. (1994). personal communication.
Farrell, P. M., MacGillivray, W. R., and Standage, M. C. (1988). *Phys. Rev.* A **37**, 4240.
Farrell, P. M., MacGillivray, W. R., and Standage, M. C. (1991). *Phys. Rev.* A **44**, 1828.
Hall, B. V., MacGillivray, W. R., and Standage, M. C. (1995). Abstracts, Advanced Workshop on Atomic and Molecular Physics, Australian National University, unpublished.
Hertel, I. V., and Stoll, W. (1974). *J. Phys.* B **7**, 583.
Hertel, I. V., and Stoll, W. (1977). *Adv. At. Mol. Phys.* **13**, 113.
Jiang, Y. T., Zuo, M., Vuskovic, L., and Bederson, B. (1992). *Phys. Rev. Lett.* **68**, 915.
Law, M. R., and Teubner, P. J. O. (1993). Abstracts, Australian Conference on Optics, Lasers and Spectroscopy, University of Melbourne, p. 290, unpublished.
McEachran, R. P. (1994). personal communication.
MacGillivray, W. R., and Standage, M. C. (1988). *Phys. Rep.* **168**, 1.
Madison, D. (1994). personal communication.

Masters, A. T., Murray, A. J., Pascual, R., and Standage, M. C. (1995). *Phys. Rev.* A, submitted.
Murray, A. J., MacGillivray, W. R., and Standage M. C. (1990). *J. Phys.* B **23**, 3373.
Murray, A. J., Pascual, R., MacGillivray, W. R., and Standage M. C. (1992). *J. Phys.* B **25**, 1915.
Murray, A. J., Webb, C. J., MacGillivray, W. R., and Standage, M. C. (1989). *Phys. Rev. Lett.* **62**, 411.
Newell, W. R. (1992). *Comm. At. Molec. Phys.* **28**, 59.
Nienhuis, G. (1980). *In* 'Coherence and Correlation in Atomic Collisions' (Eds H. Kleinpoppen and J. F. Williams), p. 121 (Plenum: New York).
Sang, R. T. (1995). PhD thesis, Griffith University.
Sang, R. T., Farrell, P. M., Madison, D., MacGillivray, W. R., and Standage, M. C. (1994). *J. Phys.* B **27**, 1187.
Srivastava, R., Zuo, T., McEachran, R. P., and Stauffer, A. D. (1992). *J. Phys.* B **25**, 2409.
Zuo, T., McEachran, R. P., and Stauffer, A. D. (1991). *J. Phys.* B **24**, 2853.

Manuscript received 14 February, accepted 6 June 1995